LOCAL CURRENT DENSITY AND CATHODIC ARC ROOT SHAPE IN A ROTATING THERMAL ARC

P.T. Eubank[1] and R.J. Munz[2]

[1] Department of Chemical Engineering, Texas A&M University
College Station, Texas, USA, 77843-3122

[2] CRTP, Department of Chemical Engineering
McGill University, 3480 University St.
Montreal, Canada, H3A 2A7

ABSTRACT

The "teepee" shape of the linear current distribution measurements of Szente at low arc velocity can be explained only by a local current density that is much more focused at the centre of the arc root than that given by the traditional Gaussian function. A current distribution function (CDF) is developed in agreement with experiment and then extended to higher velocities using a "Doorknob Model" for the shape of the arc root. Such higher focus of the current inside the arc root causes a hot spot which explains why many previous erosion models fail to forecast any erosion when erosion tracks and cathode weight loss are clearly observed.

INTRODUCTION

The local current density J_{xy} is an important parameter in determining electrode erosion in plasma torches. Szente et al [1,2,3] developed a technique which permitted the measurement of linear current densities J_x (the integral of J_{xy} over y at some x) as a rotating arc passed over a magnetic probe. The arc moved around the inner circumference of a cylindrical cathode. In this work we address the problem of modelling Szente's data [3] to produce three-dimensional current density distributions at the cathode. The experimental work was carried out with a magnetically driven arc for a variety of plasma gases at near atmospheric pressure. The arc velocity was manipulated by changing the magnetic field strength.

The local current density at the cathode surface at fixed time varies in both the direction of arc movement, x, and the transverse direction, y. It should be symmetric about $y=0$ whether the arc velocity U_x is due to fluid mechanical forces or those from an external magnetic field B (Lorentz). As the arc root velocity, U_x, approaches zero the arc foot shape must become circular with J_{xy} dependent only upon the radius, r, from the circle centre.

SHAPE OF THE CATHODE ARC ROOT USING LCD MEASUREMENTS

Figure 1 shows the general shape of the arc root on the cathode surface when the arc is moving from left to right with the current flowing into the page. The local current density J_{xy} at fixed time, t, varies in both the direction of arc movement x and the transverse direction y. J_{xy} should be symmetric about y=0. Szente measured the linear current distribution, (LCD), J_x vs x:

$$J_x \equiv 2\int_0^{a_x} J_{xy}\,dy \tag{1}$$

Here $a_x(x)$ is the vertical distance to the plasma boundary. The total current, I, is

$$I=\int_{-b_1}^{b_1}\left[2\int_0^{a_x} dy\right]dx=\int_{-b_2}^{b_1} J_x(dx) \tag{2}$$

The only weakness of the LCD method is that it cannot see a_x or $\underline{a}$. The LCD curves of Szente take two general forms as shown In Figure 2. For $B\cong 0$, (Figure 2a) near symmetry is reached in x. The maximum J_x is labelled J_{xo} at x=0. In addition, $b_1 \cong b_2 \cong a$, and J_x vs x is concave, $(d^2J_x/dx^2) > 0$.

DOORKNOB MODEL OF ARC ROOT CURRENT DISTRIBUTION

The doorknob model uses an elliptical front and a parabolic tail i.e.:

$$(a_x/a)^2 = 1-(x/b_1)^2, \qquad for\ 0<x<b_1 \tag{3}$$

$$(a_x/a) = (x-b_2)^2/b_2^2, \qquad for\ -b_2<x<0 \tag{4}$$

Its general shape agrees with the LCD measurements, high speed movies taken of the arcs, as well as the shape of fluid particles falling through stagnant fluids. The LCD curves of J_x vs x could also be empirically fit with a serpentine curve of the form: $J_x = [ABx/(A^2 + x^2)]-A$, where A and B are constants. This, however, requires a change of coordinates and causes the loss of some details in J_{xy}.

Two important yardsticks used to find the nature of J_{xy} under the doorknob geometry are: (I/J_{xo}) and (I_F/I_T) or I(front)/I(tail). Both of these parameters are easily obtained from the LCD curves of Szente. To find J_{xy} we start with Figure 2a ($B\cong 0$), where $b_1 \cong b_2 \cong a$. $J_{xo}=2\int_0^a J_{xy}\,|_{x=0}\,(dy)$ and I follows from Eq. (2). If J_{xy} = constant,

$(I/J_{xo}a)=1.57$. If J_{xy} is Gaussian, $J_{xy}=\left[J_m/(1-\frac{1}{e})\right]\left[e^{(-r/a)^2}-\left(\frac{1}{e}\right)\right]$, where $r^2=x^2+y^2$ and $J_m=J_{xy}$ (x=0,y=0) and here $(I/J_{xo}a) = 1.095$. This equation for J_{xy} can be thought of as the product of a normalization term, $\{J_m/[1-(1/e)]\}$, and the actual current distribution function, the second bracket. However from the LCD with Ar+0.3% CO at B=10 G (nearly 0), a ($\cong b_1$, $\cong b_2$) $\cong$ 3.5 mm, so $(I/J_{xo}a) = 0.80$; this means that the current distribution function (CDF) is more concentrated at the centre. Here, for x-y symmetry,

$$CDF\equiv\left[\exp\left\{-(x^2+y^2)^{\frac{n}{2}}\right\}-\frac{1}{e}\right] \tag{5}$$

where now x=(x/a) and y=(y/a) and $J_{xy} = \{J_m/[1-(1/e)]\}$(CDF). The appropriate value of n in this distribution comes from the required value of $I/J_{xo}a$, or more importantly, the value that makes the J_x vs x curves concave upwards as is observed experimentally. Varying n, we find $(I/J_{xo}a) = 0.791$ for n=0.1 and $(I/J_{xo}a) = 0.955$, n=1. The CDF curve of equation (5) is convex upwards for constant J_{xy}. For n=2(Gaussian), J_x vs x is decidedly convex for x<0.5 and then inflects near x=0.6 to become weakly concave to x=1. This convex/concave nature is retained for n=1, including a rounded top unlike Fig. 2a. Near n=0.1, this convexity near x=0 is lost. For n=0.1, the entire curve strongly resembles Fig. 2a. Since curves between n=0.1 and 0.01 are not distinguishable, a value of n=0.1 was chosen for the remainder of this work.

To find J_{xy} for current distributions of the type corresponding to Figure 2b (B>>0, U_x>>0),

$$CDF=\exp\left\{-\left[\left(\frac{x}{b_2}\right)^2+\left(\frac{y}{a}\right)^2\right]^{\frac{n}{2}}\right\}-\left(\frac{1}{e}\right) \tag{6}$$

for $-b_2<x<b_1$. Again, $J_{xy}=\{J_m/[1-(1/e)]\}$. J_x is found from Eq. (1) with a_x from doorknob equations for x<0 and for x>0. The current, I, is then found from Eq. (2). The parameter I_F/I_T is found from

$$I_F=\int_0^{b_1} J_x dx \tag{9}$$

and $I_F + I_T = I$. Exhaustive study of the Ar+0.3%CO system and other LCD curves showed that (I/J_{x0}) and (I_F/I_T) were unfortunately independent of the parameter a. We only know the parameter a near B=0, where $a\simeq b_1\simeq b_2$. Table 1 summarizes the (I/J_{xo}) and (I_F/I_T) ratios as calculated from Eq.(6). Experimental values of b_1 and b_2 were used in the model to compute (I/J_{x0}) and (I_F/I_T). The values of the parameter a

were used as given in Table 1 and are of the same order of magnitude as the zero velocity (zero magnetic field) values of b_1, defined as a_o. An important unanswered question is how does a change with B and U_x? Experimentally, b_1 can either increase or decrease with B depending upon the gas. We have used the empirical proportionality $a \propto U_x^{0.11}$ (Szente[3] using the data of Roman and Meyers[4] together with the measured U_x values (not shown on Table 1) to gently increase a with U_x and B. Again the a value is not sensitive to the ratios of Table 1 as both J_{xy} and J_m scale as the inverse of a.

Table 1
Comparison of Computed and Measured Arc Root Characteristics

System	B(G)	a_o	a(mm)	b_1 mm	b_2 mm	I/J_{xo} (mm) calc.	asp.	I_F/I_T calc.	asp.
N_2	1000	2.7	3.0	1.5	13.5	5.34	4.39	0.317	0.26
N_2	70	2.7	2.6	2.6	10.4	5.12	3.36	0.636	1.14
Ar	1000		0.6	0.4	2.4	1.05	1.26	0.45	0.31
He	120		3	2	5	2.86	2.40	0.90	0.71
He/CO	1000	1.1	1.3	2	35	11.8	9.24	0.12	0.12
He/CO	120	1.1	1.2	1.6	12.4	5.1	4.1	0.36	0.38
He/CO	60	1.1	1.1	1.3	7.75	3.36	3.04	0.44	0.39
He/N_2	800	1.2	1.8	3.4	25	-	-	-	-
He/N_2	400	1.2	1.6	2.3	21	8.28	7.97	0.312	0.33
He/N_2	120	1.2	1.4	1.5	16.5	6.27	5.14	0.26	0.22
Ar/CO	1000	3.5	4	1	16	5.70	5.30	0.185	0.136
Ar/CO	10	3.5	3.5	3.5	3.5	2.8	2.8	1	1
Avg. dev.%						20.4		19.1	

EFFECT UPON CATHODE EROSION

It is possible to examine the modelled current density distributions as they might influence electrode erosion. Two specific cases will be discussed below, both for Ar+0.3%CO. Case I is at low magnetic flux density, B=10 G, low velocity 4 m/s, and a radially symmetrical distribution of current similar to Figure 2b. Case II is at high magnetic flux density, B=1000 G, high velocity, 75 m/s, and a current distribution of the form of Figure 2b.

For Case I, $a=b_1=b_2$, so Eq.(6) with n=0.1 provides the CDF such that it drops to zero at the outer circular arc-root boundary of 3.5 mm of Figure 3a. The value of (J_{xy}/J_m) drops to 10%, for example, when the radius is 0.61 mm. We

arbitrarily define this radius as the boundary of an internal "hot spot". The hot spot carries 13.5% of the total current in a cross-sectional area that is but 3.0% of the total arc root area: the average current flux in the hot spot is 4.5 times the average for the entire arc root. When the "hot spot" is re-defined at the position where (J_{xy}/J_m) = 20%, then the hot spot radius is 0,10 mm with 0.72% of the total current but an average current flux 87 times the average for the entire arc root.

For Case II, the hot spot (returning to the original definition) is $\pm$0.60 mm for x and $\pm$0.15mm for y as shown in Fig. 3b. This hot spot was calculated using a correction factor of J_{mII}=0.53 x J_{mI} necessary to adjust the current for Case II to be the same as Case I or 140 A. Otherwise the larger total arc root area of Case II would provide a higher current and our spot size for Case II would be too large (2.84 x 0.71 mm). For moving arc roots it should be understood that Eq.(6) zeros J_{xy} only for (x,y) at $(-b_2,0)$ and $(0,+a)$; the arc-root edges along the parabola and the elliptical front have positive values of current density. At the nose $(b_1,0)$, (J_{xy}/J_m) is especially high when $b_2 >> b_1$. So while the hot spot of Fig. 3b appears inside the arc root, setting (J_{xy}/J_m) = 5% will result in a (3.14 x 0.79 mm) hot spot which overlaps b_1=1 and the nose of the arc root itself; any such model overlap must then be removed in application as no current can pass outside the doorknob boundaries of the outer arc root.

Both Case I (U_x=5 m/s) and Case II (U_x=75 m/s) provide identical erosion rates, E, of 0.4 μg/C. The cross-sectional area, A_c, of the trench cut by the moving arc is given by

$$A_c(\mu m^2) = [E(\mu g/C) \times I(A) \times 10^6/U_x(m/s) \times \rho_{Cu}(g/cm^3) \qquad (8)$$

where ρ_{Cu} is the density of copper or 8.96. A_c is then 1.25 μm^2 for Case I and 15 times less for Case II. We do not know the shape of the trench but if it is rectangular and of width similar to that of our hot spots, then the depths would be roughly two and one atomic diameters (about 0.26 nm for copper), for Cases I and II respectively. We thus suspect that our hot spots have been arbitrarily made too large ((J_{xy}/J_m) should be > 10%) and/or that the trench width is substantially less than the width of the hot spot in the y direction. The former change is not unreasonable since simple energy balances show that only 0.01 to 1% of the total current has been used to vaporize copper in Szente's experiments; for Cases I and II this figure is about 0.025%. In any event, the present CDF and Doorknob model provide reasonable boundary conditions for future heat-flux based conduction models for vaporization of cathodic electrodes. Larger values of n (>0.1) in the CDF and of the hot spot size (e.g. to include the entire arc root) only make it more difficult to explain the substantial erosion and can lead to the impossibility of subatomic erosion depths.

CONCLUSIONS

A new distribution function has been presented for the current density at the cathode surface of a thermal arc rotated by an external magnetic field. This distribution is in accord with the linear current distributions measured by Szente,

When used with an arc root model shaped like a doorknob, this distribution provides inner hot spots where the current density is many times the average value for the entire arc root. Because high local heat flux is what causes melting and then vaporization of the cathodic material, these new results can be used as boundary conditions in computer simulations for erosion without conflict with the erosion data themselves and also other physical constraints, such as those coming from energy balances and atomic erosion depths.

ACKNOWLEDGEMENTS

The financial assistance of the Natural Sciences and Engineering Research Council of Canada and Fonds pour la Formation de Chercheurs et l'Aide à la Recherche of Quebec are gratefully acknowledged.

REFERENCES

1 Szente, R.N., M.G. Drouet, and R.J. Munz, "Method to measure current distribution of an electric arc at tubular plasma torch electrodes", Review of Scientific Instruments 61(4) pp 1259-1262, April (1990)

2 Szente, R.N., M.G. Drouet, and R.J. Munz, "Current distribution of an electric arc at the surface of plasma torch electrodes", Journal of Applied Physics, 69(3), pp 1263-1268, (1991).

3 Szente, R.N.,"Erosion of plasma torch electrodes", Ph.D. thesis, McGill University, (1989)

4. W.C. Roman and T.W. Meyers, AIAA Journal, 5(11), pp 2011-2017, (1967).

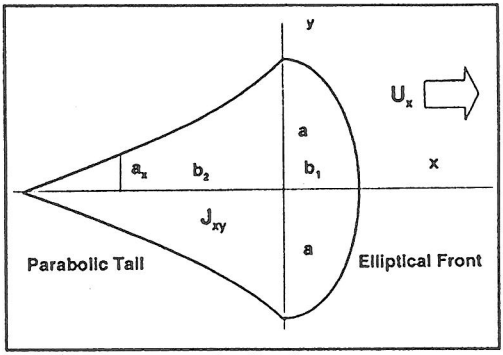

Figure 1: Current distribution at arc root

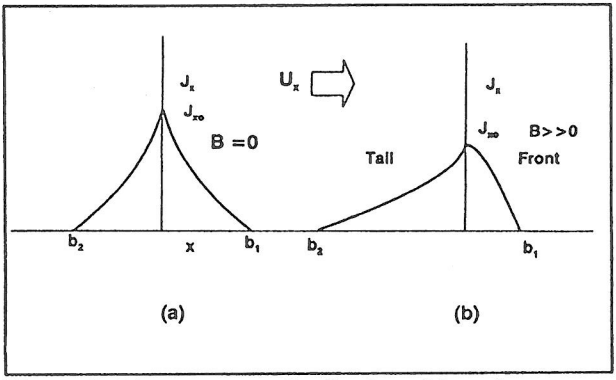

Figure 2: Linear current distributions (a) stationary, (b) moving

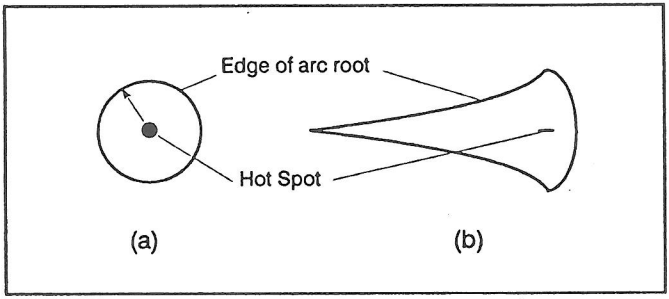

Figure 3: Outer arc roots and inner hot spots [for $(J_{xy}/J_m) > 0.1$] corresponding to Figs. 2a and 2b respectively.